3-21-2019

Partially Coherent Sources Generated from the Incoherent Sum of Fields Containing Random-width Bessel Functions

Milo W. Hyde IV
Air Force Institute of Technology

Optics Letters

Partially coherent sources generated from the incoherent sum of fields containing random-width Bessel functions

Milo W. Hyde IV

Department of Electrical and Computer Engineering, Air Force Institute of Technology, Dayton, Ohio 45433, USA (milo.hyde@us.af.mil)

Received 9 January 2019; accepted 19 February 2019; posted 25 February 2019 (Doc. ID 357253); published 21 March 2019

Using the criterion for a genuine cross-spectral density function, we demonstrate the realization of an I_m-Bessel correlated source, which has only recently been achieved using the source's coherent-mode representation. In addition, with just a simple change, we create a whole new class of partially coherent sources that have not been realized. We simulate the generation of these sources and compare the results to theoretical predictions to validate our analysis. The partially coherent sources described herein can easily be synthesized using spatial light modulators, and the approach presented in this Letter can be used to design sources for optical trapping, optical tweezers, and other related applications.

https://doi.org/10.1364/OL.44.001603

By controlling the spatial coherence of an optical source, one can significantly reduce speckle or scintillation while maintaining beam directionality. This makes spatially partially coherent beams or sources very useful in many applications (e.g., free-space optical communications, directed energy, medicine, etc.) and generally explains their popularity in the literature.

In general, there are two ways to realize a partially coherent source (PCS). The first starts with a spatially incoherent source and uses the van Cittert–Zernike theorem, or spatially filters the incoherent source to produce the desired partially coherent beam. The interested reader should consult Ref. [1] for more information on this approach.

The second technique, relevant to the work presented here, begins with a spatially coherent source and "spoils" the coherence by randomizing the field's amplitude or phase, typically using spatial light modulators (SLMs). Several different techniques have been developed to generate screens—either complex amplitude or phase—to synthesize the requisite random optical fields. These include the Monte Carlo spectral method, Cholesky factorization or decomposition, using the source's coherent-mode representation, and using the genuine cross-spectral density (CSD) function criterion derived in Ref. [2].

The Monte Carlo spectral method [3] is the most computationally efficient and therefore the most popular; unfortunately, it can be used to synthesize only uniformly correlated or Schell-model PCSs [4]. Cholesky factorization [5] can be used to synthesize any PCS with a genuine CSD function; however, it is computationally onerous—see Ref. [5] for more details. Using the source's coherent-mode representation [6] is a relatively new approach and, like Cholesky factorization, can be used to synthesize any genuine PCS. The main drawback here is that the source's coherent-mode representation must be known—the coherent modes are solutions to an integral equation [4]—and only a few have been found. Using the genuine CSD criterion is also a relatively new synthesis approach [7] and, like the two prior methods, can be used to generate any genuine PCS. Although the genuine CSD criterion is an integral equation, its form generally allows one to use intuition to develop functions for the criterion's constituents (discussed later) that satisfy it.

In this Letter, we use the genuine CSD criterion approach to generate a PCS—an I_m-Bessel correlated beam [8]—that has only recently been realized using the source's coherent-mode representation [6]. With just a simple change, we generalize the results in Refs. [6,8] to create a whole new class of PCSs that do not have closed-form coherent-mode representations and have not been realized. To validate our approach, we simulate the generation of an I_m-Bessel correlated source and compare the results to the corresponding theoretical expressions. We also simulate the generation of a new source—one that has not been realized—and perform the same comparisons. We lastly conclude this Letter with a summary of the work presented herein and a brief discussion of potential applications.

We start with the sufficient condition for a genuine CSD function W:

$$W(\boldsymbol{\rho}_1,\boldsymbol{\rho}_2) = \iint_{-\infty}^{\infty} p(\boldsymbol{v}) H(\boldsymbol{\rho}_1,\boldsymbol{v}) H^*(\boldsymbol{\rho}_2,\boldsymbol{v}) \mathrm{d}^2 v, \quad (1)$$

where $\boldsymbol{v} = \hat{\boldsymbol{x}} v_x + \hat{\boldsymbol{y}} v_y$, $\boldsymbol{\rho} = \hat{\boldsymbol{x}} x + \hat{\boldsymbol{y}} y$, H is an arbitrary kernel, and p is a non-negative function [2]. The dependence of the functions in Eq. (1) on radian frequency ω has been omitted for brevity.

Although H is a purely mathematical construct, here we physically interpret it as a realization of an optical field drawn from a random process [7]. For example, let $H(\boldsymbol{\rho},\boldsymbol{v}) = \tau(\boldsymbol{\rho}) \exp(j\boldsymbol{v}\cdot\boldsymbol{\rho})$, where τ is a complex function. This choice of H produces Schell-model sources [2,4].

Interpreting H in this manner means that τ is physically the field's complex, deterministic amplitude, and the exponential function is the field's random phase. For Schell-model sources, the field's phase is a randomly tilted phase front, where $\boldsymbol{v}$ is a random slope. The function p in Eq. (1) is the joint probability density function (PDF) of the x and y slopes. This approach has been used to simulate [9] and physically realize Schell-model sources using only a fast steering (tip-tilt) mirror [10]. We note that by changing the exponential function from random tilt to random defocus, nonuniformly correlated beams can be generated as well [7,11–14].

Here, we let

$$H(\boldsymbol{\rho}, v) = \tau(\boldsymbol{\rho}) J_m(\rho v), \tag{2}$$

where J_m is an mth-order Bessel function of the first kind; m is not necessarily an integer, yet we do assume that $m \geq 0$; $\rho = |\boldsymbol{\rho}|$; and $v = |\boldsymbol{v}|$. Substituting the above H into Eq. (1) and simplifying produces

$$W_{J_m}(\boldsymbol{\rho}_1, \boldsymbol{\rho}_2) = \tau(\boldsymbol{\rho}_1)\tau^*(\boldsymbol{\rho}_2) \iint_{-\infty}^{\infty} p(\boldsymbol{v}) J_m(\rho_1 v) J_m(\rho_2 v) \mathrm{d}^2 v. \tag{3}$$

Assuming that p is rotationally invariant, transforming the integrals into polar coordinates, and evaluating the trivial integral over angle yields

$$W_{J_m}(\boldsymbol{\rho}_1, \boldsymbol{\rho}_2) = \tau(\boldsymbol{\rho}_1)\tau^*(\boldsymbol{\rho}_2) 2\pi \int_0^{\infty} v p(v) J_m(\rho_1 v) J_m(\rho_2 v) \mathrm{d}v. \tag{4}$$

Note that Eq. (4) gives rise to a whole family of PCSs that can be synthesized by incoherently summing beams composed of mth-order Bessel functions with random widths v drawn from joint PDF p. Due to the J_m, these sources generally have an annular shape with a dark center—the exception being the $m = 0$ case, which has a bright center. Depending on τ and p, the CSD function W_{J_m} can be made shape invariant [8,15]. These characteristics make these sources potentially useful in applications involving optical trapping or optical tweezers.

We begin by showing that the family of PCSs described by W_{J_m} includes I_m-Bessel correlated beams [8], which have only recently been synthesized [6]. Let p take a Gaussian form, namely,

$$p_{\mathrm{G}}(v) = \frac{\delta^2}{\pi} \exp(-\delta^2 v^2), \tag{5}$$

where δ is a positive constant and physically the source's correlation or coherence radius. The constant in front of the exponential is there to ensure that the joint PDF p_{G} integrates to one.

The integral in Eq. (4), with p_{G} substituted in, can be found in Ref. [18]:

$$W_{J_m\mathrm{G}}(\boldsymbol{\rho}_1, \boldsymbol{\rho}_2) = \tau(\boldsymbol{\rho}_1)\tau^*(\boldsymbol{\rho}_2) \exp\left(-\frac{\rho_1^2 + \rho_2^2}{4\delta^2}\right) I_m\left(\frac{\rho_1 \rho_2}{2\delta^2}\right), \tag{6}$$

where I_m is an mth-order modified Bessel function of the first kind. The CSD function of an I_m-Bessel correlated source is

$$W_{I_m}(\boldsymbol{\rho}_1, \boldsymbol{\rho}_2) = \frac{\xi^{-m/2}}{1-\xi} \exp\left(-\frac{1+\xi}{1-\xi}\frac{\rho_1^2 + \rho_2^2}{\sigma^2}\right) \times \exp[-jm(\phi_1 - \phi_2)] I_m\left(\frac{4\sqrt{\xi}}{1-\xi}\frac{\rho_1 \rho_2}{\sigma^2}\right), \tag{7}$$

where σ is the source's size, and $0 < \xi < 1$ is a measure of the spatial coherence of the field—$\xi \to 0$ is a coherent field, and $\xi \to 1$ corresponds to an incoherent field [6,8].

Comparing Eqs. (6) and (7) reveals the following:

$$\delta = \sqrt{\frac{\sigma^2}{8}\frac{1-\xi}{\sqrt{\xi}}},$$
$$\tau(\boldsymbol{\rho}) = \sqrt{\frac{\xi^{-m/2}}{1-\xi}} \exp(-jm\phi) \exp\left[-\frac{(1-\sqrt{\xi})^2}{1-\xi}\frac{\rho^2}{\sigma^2}\right]. \tag{8}$$

Substituting the above τ into Eq. (2) gives the stochastic optical field instance that produces an I_m-Bessel correlated source, namely,

$$U_{I_m}(\boldsymbol{\rho}) = \sqrt{\frac{\xi^{-m/2}}{1-\xi}} \exp(-jm\phi) \exp\left[-\frac{(1-\sqrt{\xi})^2}{1-\xi}\frac{\rho^2}{\sigma^2}\right] J_m(\rho v), \tag{9}$$

where v is a random number drawn from the following joint Gaussian PDF:

$$p_{\mathrm{G}}(v_x, v_y) = \frac{\sigma^2}{8\pi}\frac{1-\xi}{\sqrt{\xi}} \exp\left[-\frac{\sigma^2}{8}\frac{1-\xi}{\sqrt{\xi}}(v_x^2 + v_y^2)\right]. \tag{10}$$

Note that p_{G} is separable in v_x and v_y, and thus, v_x and v_y are independent, identically distributed, Gaussian random numbers. Field instances given by Eq. (9) can easily be synthesized using SLMs [16].

Choosing another positive, normalized function or PDF for p produces a different PCS. Here, as an example, we choose a circular p [a two-dimensional (2D) uniform distribution], i.e.,

$$p_{\mathrm{U}}(v) = \frac{\delta^2}{\pi}\mathrm{circ}(\delta v), \tag{11}$$

where $\mathrm{circ}(x)$ is the circle function defined in Ref. [17], and δ has the same physical interpretation as in Eq. (5). Substituting Eq. (11) into Eq. (4) produces

$$W_{J_m\mathrm{U}}(\boldsymbol{\rho}_1, \boldsymbol{\rho}_2) = \tau(\boldsymbol{\rho}_1)\tau^*(\boldsymbol{\rho}_2) 2\delta^2 \int_0^{1/\delta} v J_m(\rho_1 v) J_m(\rho_2 v) \mathrm{d}v. \tag{12}$$

The above integral can be found in Ref. [18] when $\rho_1 \neq \rho_2$:

$$W_{J_m\mathrm{U}}(\boldsymbol{\rho}_1, \boldsymbol{\rho}_2) = \tau(\boldsymbol{\rho}_1)\tau^*(\boldsymbol{\rho}_2) \times 2\frac{\frac{\rho_2}{\delta} J_m\left(\frac{\rho_1}{\delta}\right) J_{m-1}\left(\frac{\rho_2}{\delta}\right) - \frac{\rho_1}{\delta} J_{m-1}\left(\frac{\rho_1}{\delta}\right) J_m\left(\frac{\rho_2}{\delta}\right)}{\left(\frac{\rho_1}{\delta}\right)^2 - \left(\frac{\rho_2}{\delta}\right)^2}. \tag{13}$$

When $\rho_1 = \rho_2 = \rho$, the integral in Eq. (12) can be evaluated using Mellin transforms and the Mellin convolution theorem [19]. First, we rewrite Eq. (12) as

$$W_{J_m\mathrm{U}}(\rho, \phi_1; \rho, \phi_2) = \tau(\rho, \phi_1)\tau^*(\rho, \phi_2) 2 \int_0^{\infty} \frac{\mathrm{d}v}{v} v^2 \theta(1-v) J_m^2\left(\frac{\rho}{\delta} v\right), \tag{14}$$

where θ is the Heaviside unit step function. Substituting in the Mellin transforms for the functions in the integrand and simplifying produces

$$W_{J_m\mathrm{U}}(\rho,\phi_1;\rho,\phi_2) = \tau(\rho,\phi_1)\tau^*(\rho,\phi_2) \times \frac{1}{\sqrt{\pi}}\frac{1}{j2\pi}\int_C \left(\frac{\delta}{\rho}\right)^{-2s} \frac{\Gamma(m-s)\Gamma(s+1/2)}{\Gamma(s+2)\Gamma(s+m+1)}\,\mathrm{d}s, \quad (15)$$

where Γ is the gamma function, and C is the integration path in the complex s plane shown in Fig. 1. The integrand has simple poles at $s = n + m$ and $s = -n - 1/2$, where $n = 0, 1, 2, \ldots$, due to the numerator gamma functions. Examining the asymptotic behavior of the integrand reveals that the integral should be closed in the right-half plane. The integration contour encloses the $s = n + m$ poles, and by Cauchy's residue theorem, Eq. (15) becomes

$$W_{J_m\mathrm{U}}(\rho,\phi_1;\rho,\phi_2) = \tau(\rho,\phi_1)\tau^*(\rho,\phi_2)\frac{[\rho^2/(4\delta^2)]^m}{\Gamma(m+1)\Gamma(m+2)} \times {}_1F_2(m+1/2; m+2, 2m+1; -\rho^2/\delta^2), \quad (16)$$

where ${}_1F_2$ is a generalized hypergeometric function. Thus,

$$W_{J_m\mathrm{U}}(\boldsymbol{\rho}_1,\boldsymbol{\rho}_2) = \begin{cases} \text{Eq. (13)} & \rho_1 \neq \rho_2 \\ \text{Eq. (16)} & \rho_1 = \rho_2 = \rho \end{cases}. \quad (17)$$

The field that produces this source is

$$U_{J_m\mathrm{U}}(\boldsymbol{\rho}) = \tau(\boldsymbol{\rho})J_m(\rho v), \quad (18)$$

where v is a random number drawn from the PDF in Eq. (11). We note that Eq. (12) can be evaluated directly using Mellin transform techniques. The result is a double Taylor series that converges for all values of ρ_1, ρ_2, δ. Numerically computing $W_{J_m\mathrm{U}}$ using this relation is very slow, and therefore, we use Eq. (17).

To verify the above analysis, we present simulation results where we generated the above PCSs. Before proceeding to the results, we briefly discuss the setup. For the simulations, we used 512×512 computational grids; the grid spacing was 15.38 μm. We generated 100,000 realizations of the optical fields given in Eqs. (9) and (18) to compute 2D "cuts" through the four-dimensional (4D) CSD functions in Eqs. (7) and (17), respectively. To remain consistent with the I_m-Bessel correlated source, we chose the same δ and τ given in Eq. (8) for the PCS in Eq. (17). The ξ, m, and σ were 0.25 mm, 3 mm, and 1 mm, respectively.

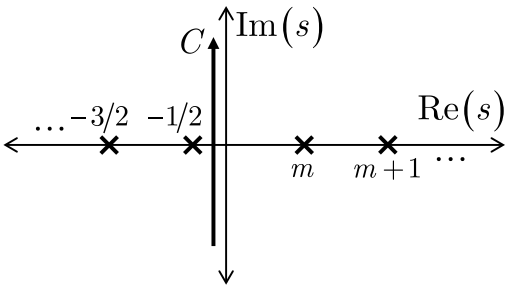

Fig. 1. Complex s plane corresponding to Eq. (15).

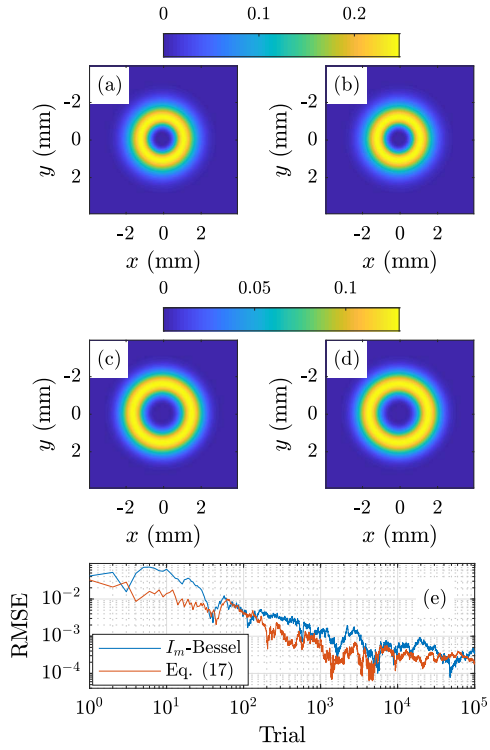

Fig. 2. Spectral density $S(\boldsymbol{\rho}) = W(\boldsymbol{\rho},\boldsymbol{\rho})$ results: (a) I_m-Bessel theory, (b) I_m-Bessel simulation, (c) Eq. (17) theory, (d) Eq. (17) simulation, and (e) RMSEs for the simulated I_m-Bessel (blue trace) and Eq. (17) sources (red trace) versus trial number.

Figure 2 shows the spectral density $S(\boldsymbol{\rho}) = W(\boldsymbol{\rho},\boldsymbol{\rho})$ [4] results: (a) and (b) show the theoretical and simulated results for the I_m-Bessel correlated source, and (c) and (d) show the same results for the Eq. (17) source. Figure 2(e) shows the

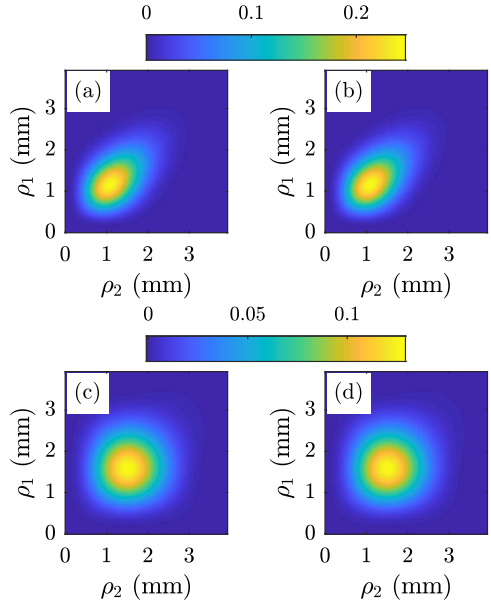

Fig. 3. $W(\rho_1,\phi;\rho_2,\phi)$ results versus ρ_1 and ρ_2: (a) I_m-Bessel theory, (b) I_m-Bessel simulation, (c) Eq. (17) theory, and (d) Eq. (17) simulation.

root-mean-square errors (RMSEs) for the simulated I_m-Bessel and Eq. (17) sources versus trial number:

$$\mathrm{RMSE} = \sqrt{\frac{1}{N^2}\sum_{k=1}^{N^2}\left(S^{\mathrm{sim}}[k] - S^{\mathrm{thy}}[k]\right)^2}, \tag{19}$$

where k is a pixel index, and the sum is over all $N^2 = 512^2$ pixels. Overall, the simulated results are in excellent agreement with the theoretical spectral densities. Figure 2(e) shows that convergence to the theoretical spectral densities occurs rather quickly, i.e., within 500–1000 field realizations.

Figure 3 shows $W(\rho_1, \phi; \rho_2, \phi)$ plotted versus ρ_1 and ρ_2 for both sources. The layout of the figure is identical to Fig. 2, with the exception of Fig. 2(e). The RMSE results here are similar to those in Fig. 2(e) and thus are omitted for brevity. Again, the agreement between theory and simulation is excellent. These results show an example of where these similar sources differ.

Lastly, Fig. 4 shows the magnitudes (top of each subfigure) and phases (bottom of each subfigure) of $W(x_1, y_1; \ell, 0)$, where $\ell = 1.15$ mm and 1.55 mm for the I_m-Bessel correlated [theory (a) and simulation (b)] and Eq. (17) [theory (c) and simulation (d)] sources, respectively. These (x_2, y_2) points lie approximately on the maxima of the "rings" in Fig. 2. The results clearly show that the sources' phase vortices are accurately produced. The disagreements between the theoretical and simulated I_m-Bessel source phases [(a) and (b), respectively] occur in "low-intensity" regions and are numerical in nature.

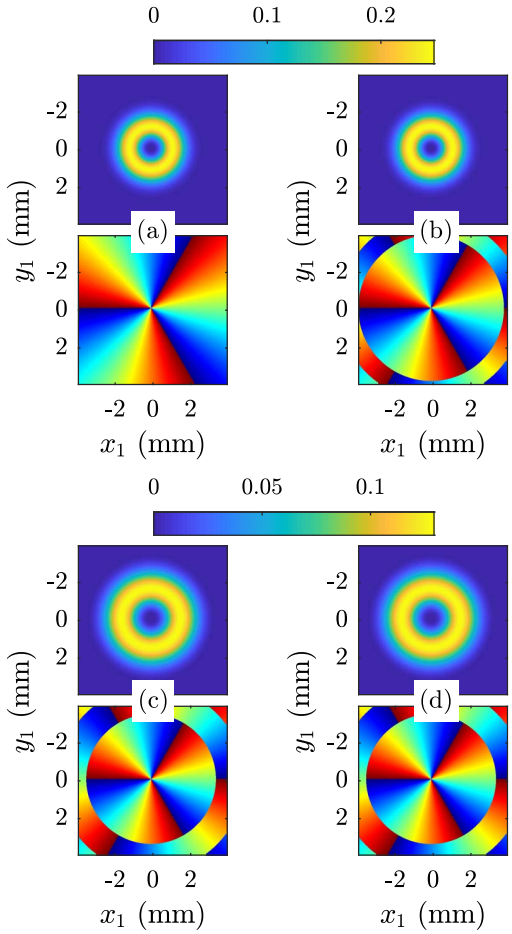

Fig. 4. Magnitude (top) and phase (bottom) of $W(x_1, y_1; \ell, 0)$ versus x_1 and y_1: (a) I_m-Bessel theory, (b) I_m-Bessel simulation, (c) Eq. (17) theory, and (d) Eq. (17) simulation. For the I_m-Bessel source, $\ell = 1.15$ mm, and for the Eq. (17) source, $\ell = 1.55$ mm. The color bars above (a) and (b), and (c) and (d) correspond to the I_m-Bessel and Eq. (17) magnitude results, respectively. All the phase results are plotted on the same $(-\pi, \pi]$ color scale.

In conclusion, applying the genuine CSD criterion, we developed a method to generate PCSs by incoherently summing beams composed of Bessel functions with random widths. The PDF of the Bessel function width determined the source. By choosing a Gaussian PDF, we showed that this new class of PCSs included I_m-Bessel correlated sources, which have only recently been synthesized using the source's coherent-mode representation. We then derived the CSD function for a new source, one that has not been realized, simply by changing the random-width PDF from Gaussian to uniform. To validate our analysis, we simulated the generation of an I_m-Bessel correlated source and the new PCS. We compared simulated 2D slices of the 4D CSDs to the corresponding theory. The simulated and theoretical results were in excellent agreement.

The family of PCSs developed in this Letter—being composed of Bessel-beam-like fields—can easily be synthesized using SLMs. These sources' annular shapes and shape invariances make them (and hence the synthesis technique described herein) potentially useful in optical trapping, optical tweezers, and other related applications.

Acknowledgment. The views expressed in this Letter are those of the authors and do not reflect the official policy or position of the U.S. Air Force, the Department of Defense, or the U.S. Government.

REFERENCES

1. Y. Cai, Y. Chen, J. Yu, X. Liu, and L. Liu, Prog. Opt. **62**, 157 (2017).
2. F. Gori and M. Santarsiero, Opt. Lett. **32**, 3531 (2007).
3. C. A. Mack, Appl. Opt. **52**, 1472 (2013).
4. L. Mandel and E. Wolf, *Optical Coherence and Quantum Optics* (Cambridge University, 1995).
5. M. W. Hyde IV, S. Bose-Pillai, D. G. Voelz, and X. Xiao, Phys. Rev. Appl. **6**, 064030 (2016).
6. X. Chen, J. Li, S. M. H. Rafsanjani, and O. Korotkova, Opt. Lett. **43**, 3590 (2018).
7. M. W. Hyde IV, S. Bose-Pillai, X. Xiao, and D. G. Voelz, J. Opt. **19**, 025601 (2017).
8. S. A. Ponomarenko, J. Opt. Soc. Am. A **18**, 150 (2001).
9. G. J. Gbur, Opt. Express **14**, 7567 (2006).
10. M. W. Hyde IV, S. R. Bose-Pillai, X. Xiao, and D. G. Voelz, Microw. Opt. Technol. Lett. **59**, 2731 (2017).
11. Y. Gu and G. Gbur, Opt. Lett. **38**, 1395 (2013).
12. M. W. Hyde IV, S. R. Bose-Pillai, and R. A. Wood, Appl. Phys. Lett. **111**, 101106 (2017).
13. M. W. Hyde IV and S. R. Bose-Pillai, Opt. Lett. **42**, 3084 (2017).
14. M. Santarsiero, R. Martínez-Herrero, D. Maluenda, J. C. G. de Sande, G. Piquero, and F. Gori, Opt. Lett. **42**, 4115 (2017).
15. F. Gori, Opt. Commun. **46**, 149 (1983).
16. X. Yu, A. Todi, and H. Tang, Appl. Opt. **57**, 4677 (2018).
17. J. W. Goodman, *Introduction to Fourier Optics*, 3rd ed. (Roberts & Company, 2005).
18. I. S. Gradshteyn and I. M. Ryzhik, *Table of Integrals, Series, and Products*, 7th ed. (Academic, 2007).
19. R. J. Sasiela, *Electromagnetic Wave Propagation in Turbulence: Evaluation and Application of Mellin Transforms*, 2nd ed. (SPIE, 2007).